Synthesis of Novel Lignin-Based Ion-Exchange Resin and Its Utilization in Heavy Metals Removal

ARTICLE *in* INDUSTRIAL & ENGINEERING CHEMISTRY RESEARCH · JANUARY 2013

Impact Factor: 2.59 · DOI: 10.1021/ie301863e

5 AUTHORS, INCLUDING:

Fengbing Liang
Qingdao Institute of Bioenergy and Bioproces…
7 PUBLICATIONS **35** CITATIONS

SEE PROFILE

I&EC research
Industrial & Engineering Chemistry Research

Article

pubs.acs.org/IECR

Synthesis of Novel Lignin-Based Ion-Exchange Resin and Its Utilization in Heavy Metals Removal

Feng-Bing Liang, Yan-Lei Song, Chong-Pin Huang,* Ying-Xia Li, and Biao-Hua Chen

State Key Laboratory of Chemical Resource Engineering, Beijing University of Chemical Technology, Beijing 100029, People's Republic of China

ABSTRACT: A new lignin-based resin (LBR) was prepared by condensation polymerization of sodium lignosulfonate with glucose under acidic conditions. The physical and chemical properties of LBR were characterized by scanning electron microscopy (SEM), X-ray diffraction (XRD), X-ray photoelectron spectroscopy (XPS), Fourier transform infrared (FTIR) spectroscopy, thermogravimetric analysis (TGA), and ^{13}C cross-polarization magic angle spinning nuclear magnetic resonance (^{13}C CP MAS NMR). Structure analyses revealed that the resulting spherical particles are composed of amorphous cross-linked phenylpropane-based polymers that have a high density of acidic groups and high thermal stability. The adsorption performance of heavy metals (Cr(III), Cu(II), Ni(II), Pb(II), and Cd(II)) onto LBR were investigated. Langmuir, Freundlich, and Dubinin−Radushkevich (D-R) models were applied to analyze the experimental data. The maximum adsorption capacity of LBR for the five metals was in the following order: Pb(II) ≫ Cu(II) > Cd(II) > Ni(II) ≈ Cr(III). The experimental data were also tested by pseudo-first-order, pseudo-second-order, and intraparticle diffusion kinetic models. The adsorption process of all metal ions on LBR is well-described by the pseudo-second-order model. Moreover, the regeneration method of LBR was also studied.

1. INTRODUCTION

Ion-exchange resins have a wide range of applications in separation, purification, decontamination, and catalysis.[1−4] The ion-exchange resin typically refers to an organic polymer that exchanges ions with a solution. Most conventional ion-exchange resins are synthesized from hydrocarbon monomers (such as styrene and divinylbenzene) by copolymerization. With the depletion of fossil fuels, the cost of resin material derived from hydrocarbon feedstocks can be expected to increase in the foreseeable future. Thus, new ion-exchange materials derived from renewable resources should be urgently required.

Biomass is a renewable resource that can be used for the production of many fuels and chemicals that are currently produced from natural gas and other fossil fuels. For example, lignins—one of the main constituents of lignocellulosic biomass (15−30% by weight)—are complex, amorphous, three-dimensional (3D) polymers that have a phenylpropane moiety as a common structural feature.[5] However, compared with cellulose biomass, valorization of lignin has received little attention. For example, lignosulfonates (LSs) are water-soluble anionic polyelectrolyte polymers that are byproducts from the production of wood pulp using sulfite pulping. The global production of lignosulfonate is currently ∼1.1 million tons per annum,[6] yet the markets for lignin-based products remain restricted and focus on low value products (e.g., dispersants, binders, and adhesives). Nevertheless, by virtue of its unique structure and chemical properties, lignin has significant potential as a source of a wide variety of bulk and fine chemicals.

The preparation of ion-exchange resins from lignosulfonate precursors has been studied since the 1950s. In early work, amorphous gel-type resins with low exchange capacities were synthesized by the polymerization of lignosulfonic acid with formaldehyde.[7] Subsequently, spherical lignin-based ion-exchange resins were prepared by reverse-phase suspension polymerization with LSs, and the ion-exchange capacity increased to 2.1−3.3 mmol/g.[8,9] Herein, this paper reports the synthesis and characterization of a lignin-based resin (LBR) with a high density of acidic groups and discusses its adsorption performance as a novel stable adsorbent in metal ions separation. The strategy adopted for the synthesis of this new type of resin involves the condensation polymerization of sodium lignosulfonate (SLS) with glucose to give a cross-linked macromolecule. This approach is simple and allows LSs to be easily converted to a practical ion-exchange resin.

2. EXPERIMENTAL SECTION

2.1. Synthesis of LBR. In a typical synthesis, SLS (20 g) and glucose (1 g) were heated at 463 K in dilute sulfuric acid (4.5%, 200 mL) in a batch reactor. After heating for 24 h, excess solution was removed from the dark solid by vacuum filtration. The resulting material was then ground to a powder and was washed repeatedly in boiling water until impurities such as sulfate ions were no longer detected in the wash water.

2.2. Analytical Methods. Structural information of LBR was characterized by scanning electron microscopy (SEM) (Veeco Model DI), powder X-ray diffraction (XRD) (Bruker, Model D8FOCUS), X-ray photoelectron spectroscopy (XPS) (ThermoFisher Scientific, Model ESCALAB-250), Fourier transform infrared (FTIR) spectroscopy (Bruker, Model TENSOR 27), thermogravimetric analysis (TGA) (Setaram, Model LCT1390-8), Brunauer−Emmett−Teller (BET) surface area measurements (Thermo Electron Corporation, Model

Received: July 15, 2012
Revised: December 12, 2012
Accepted: December 24, 2012
Published: December 24, 2012

dx.doi.org/10.1021/ie301863e | *Ind. Eng. Chem. Res.* 2013, 52, 1267−1274

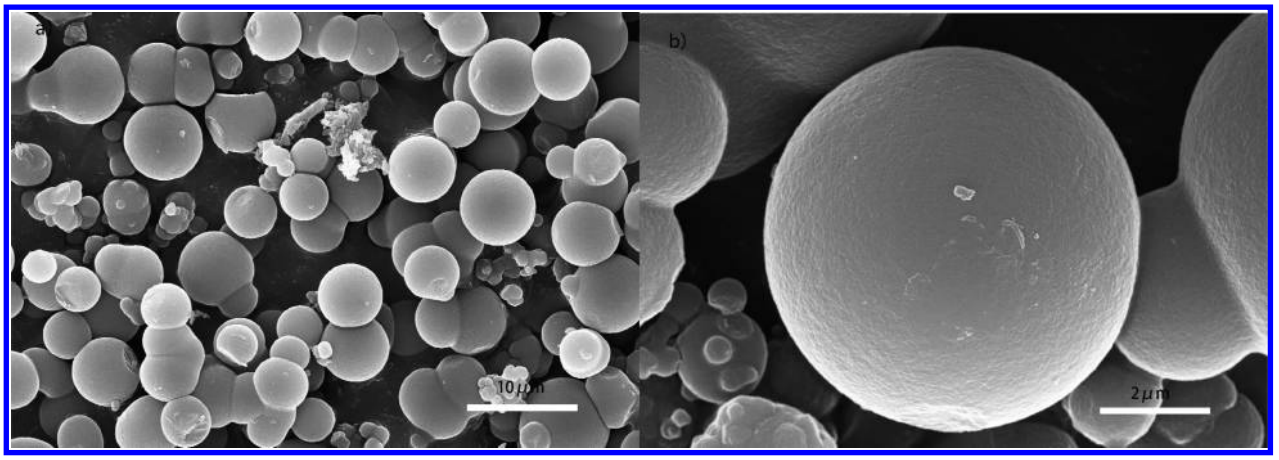

Figure 1. Scanning electron microscopy (SEM) images of the resulting lignin-based material.

SORPTOMATIC 1990), and ^{13}C cross-polarization (CP) magic angle spinning (MAS) nuclear magnetic resonance (NMR) (Bruker, Model AV300). FTIR spectra were obtained using a KBr pellet containing powdered samples with a wavenumber between 400 cm^{-1} and 4000 cm^{-1}. The amount of all of the functional groups on the surface of the prepared samples was estimated using the Boehm titration.[10,11]

2.3. Adsorption Experiments. The actual application of LBR was demonstrated through the adsorption of Cr(III), Cu(II), Ni(II), Pb(II), and Cd(II). The stock solutions of metal salts (1000 mg/L) were prepared by dissolving $Cr(NO_3)_3{\cdot}9H_2O$, $Cu(NO_3)_2{\cdot}3H_2O$, $Ni(NO_3)_2{\cdot}6H_2O$, $Pb(NO_3)_2$, and $CdCl_2{\cdot}2.5H_2O$ in deionized water. The synthetic wastewater solutions were then obtained by dilution of the stock solutions of each metal, using deionized water. Batch experiments were conducted in 150-mL Erlenmeyer flasks using 50 mL of metal ion solutions (200 mg/L) at room temperature to determine the effects of pH on the adsorption of heavy-metal ions. The pH value of the solution was adjusted to a predetermined value using 1 mol/L HCl or NaOH, and the required mass of LBR was added to the solution. The resulting suspension was stirred for a specified time in a magnetic stirrer at 150 rpm while keeping the constant pH value measured by pH meter. At the end of each experiment, the solutions were separated by filtration (0.22-μm pore-size filters). The filtrate was then analyzed for residual metal ions by inductively coupled plasma−mass spectrometry (ICP-MS). The removal efficiency (E) and adsorption capacity (q) were calculated according to eqs 1 and 2, respectively.

$$E\ (\%) = \frac{C_0 - C_i}{C_0} \times 100 \tag{1}$$

$$q\ (\mathrm{mg/g}) = \frac{V(C_0 - C_i)}{M} \tag{2}$$

where V is the volume of metal ion solution (L); C_0 and C_i are the initial and final concentrations of metal ions in solution (mg/L), respectively; and M is the mass of LBR (g). All tests were conducted in triplicate, and their mean values (the accuracy is considered to be ±5%) were used in analyzing the data. All of the reagents were purchased at high purity (AR grade) from Beijing Chemical Reagent Company.

2.4. Desorption and Regeneration Experiments. To investigate the reusability of LBR, desorption and regeneration experiments were conducted. For the desorption experiments, LBR loaded with heavy metals was transferred into 50 mL of 0.5 mol/L HCl solution while stirring at 150 rpm for 1 h at room temperature. The metal concentrations in the solution were also determined by ICP-MS. After desorption, the LBR beads were repeatedly washed with deionized water and then dried for reuse. Four adsorption−desorption cycles for each metal were conducted, and, in each cycle, the initial metals concentration was 200 mg/L. The eluted metal per gram of LBR (q_{des}) and desorption efficiency (D) were calculated using eqs 3 and 4, respectively.

$$q_{des} = C_{des}\left(\frac{V}{M}\right) \tag{3}$$

$$D\ (\%) = \frac{q_{des}}{q_{ads}} \times 100 \tag{4}$$

where V is the volume of the solution (L), C_{des} the final concentration of metal ions in solution (mg/L), and M the mass of LBR (g).

3. RESULTS AND DISCUSSION

3.1. Morphology and Properties of LBR. Figures 1a and 1b show SEM images of the resulting sample powder. The microporous material containing pores with diameters of <1 nm exists as spherical beads with grain sizes of >1 μm. The powders can easily be dispersed in water under stirring, and then be precipitated when solution stirring is stopped. In addition, the prepared samples with a nominal composition of $CH_{0.708}O_{0.144}$ were insoluble in water, even at boiling temperature.

3.2. Structures of LBR. LBR can be readily prepared by heating SLS and sugars in acidic solution at 453−473 K. As seen in Figure 3a, the FTIR spectrum of LBR shows that several functional groups (e.g., hydroxyl, ether C−O−C, and carboxyl groups) are present on the surface of LBR. There are some appreciable differences between FTIR spectra for SLS before and after polycondensation. The bands of 1219 and 1386 cm^{-1}, corresponding to the stretching vibration of the SO_3H groups, disappeared after the reaction, indicating that the desulfonated lignosulfonates were obtained in the reaction process. The absorbance at 1033 cm^{-1} is the C−O−C stretching vibration of lignin-carbohydrate complexes derived from acetylation of desulfonated lignosulfonates with carbohydrates and their derivatives. The new bands at 1260, 1439, and 1696 cm^{-1} are assigned to coupled C(═O)−O stretching

dx.doi.org/10.1021/ie301863e | Ind. Eng. Chem. Res. 2013, 52, 1267−1274

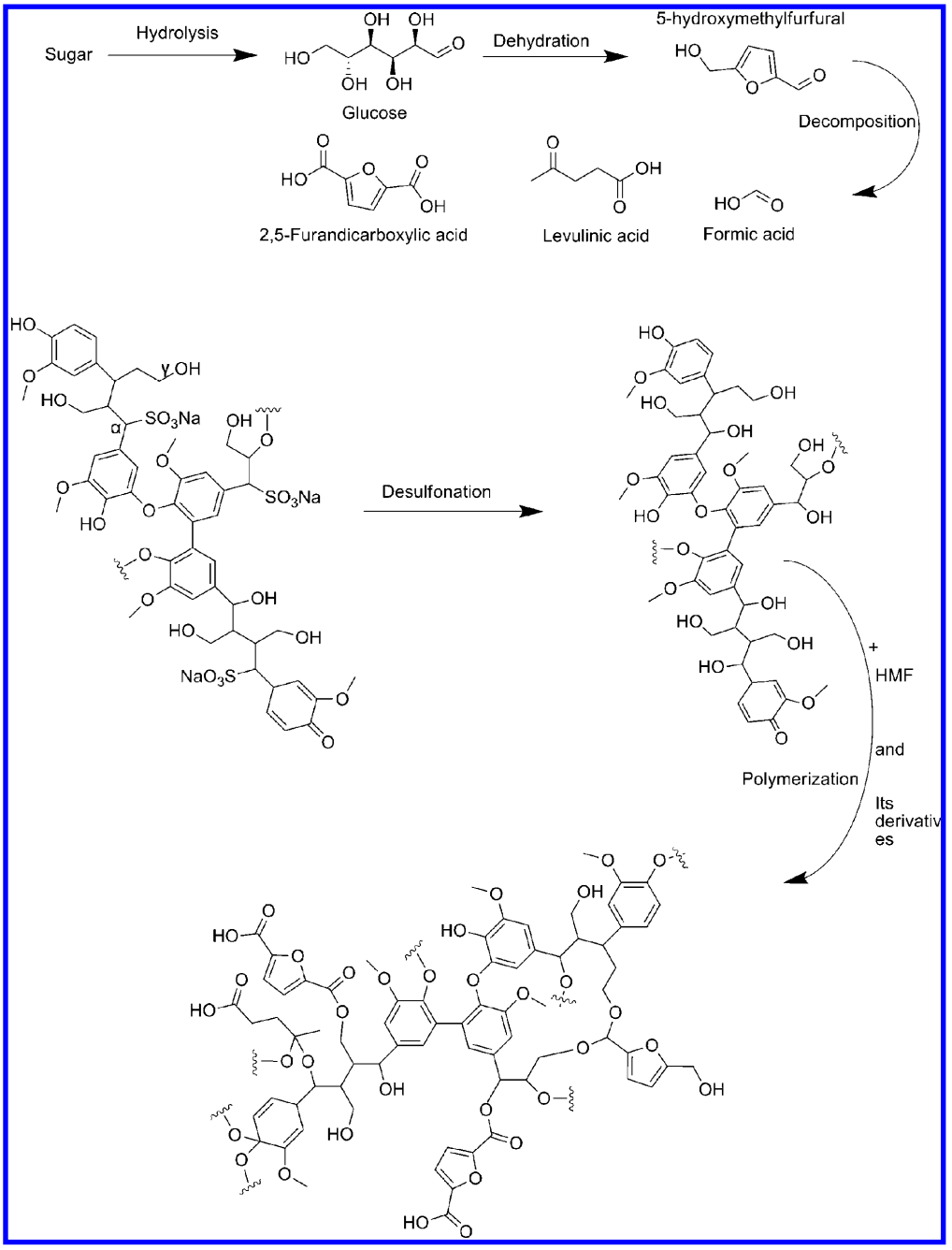

Figure 2. Possible mechanism for the formation of LBR.

vibration, OH in-plane deformation vibrations, and C=O stretching of COOH groups, respectively, indicating that carboxyl acid groups were added to the lignin to form LBR. The ^{13}C MAS NMR spectra of SLS and LBR are also shown in Figure 3b. The NMR spectrum for SLS sample consists of many peaks, which are due to OCH_3 (56 ppm), C_γ–OH (62 ppm), Ar–C_α–SO_3H, and carbohydrates (73 ppm), aromatic carbon (103–140 ppm), phenolic OH (150 ppm), and C=O (181 ppm).[12,13] After polymerization, the signals at 62, 73, and 181 ppm are not observed in the NMR spectrum of LBR. The significant differences between SLS and LBR indicate that some groups, such as C_γ–OH, Ar–C_α–SO_3H, and carbonyl groups, participated in polymerization.

According to the aforementioned analysis, possible formation pathway of LBR is shown in Figure 2. Under the experimental conditions, 5-hydroxymethylfurfural (5-HMF) was made from glucose and other sugars from raw lignin sulfonate. Once formed, HMF converts to levulinic acid under harsh conditions (high temperature, high acid concentration) in the presence of water.[14] The analysis results on the compositions of residual solution of the reaction by liquid chromatography–mass spectrometry (LC-MS) indicated the presence of levulinic acid. Under the same reaction conditions, desulfonated LSs were obtained by desulfonation of SLS. Therefore, the polymerization of LBR can take place via acetylation of desulfonated LSs with HMF and its derivatives. Especially, the reaction between desulfonated LSs with levulinic acid leads to the production of a significant amount of carboxylic acids attached to LBR.

dx.doi.org/10.1021/ie301863e | Ind. Eng. Chem. Res. 2013, 52, 1267–1274

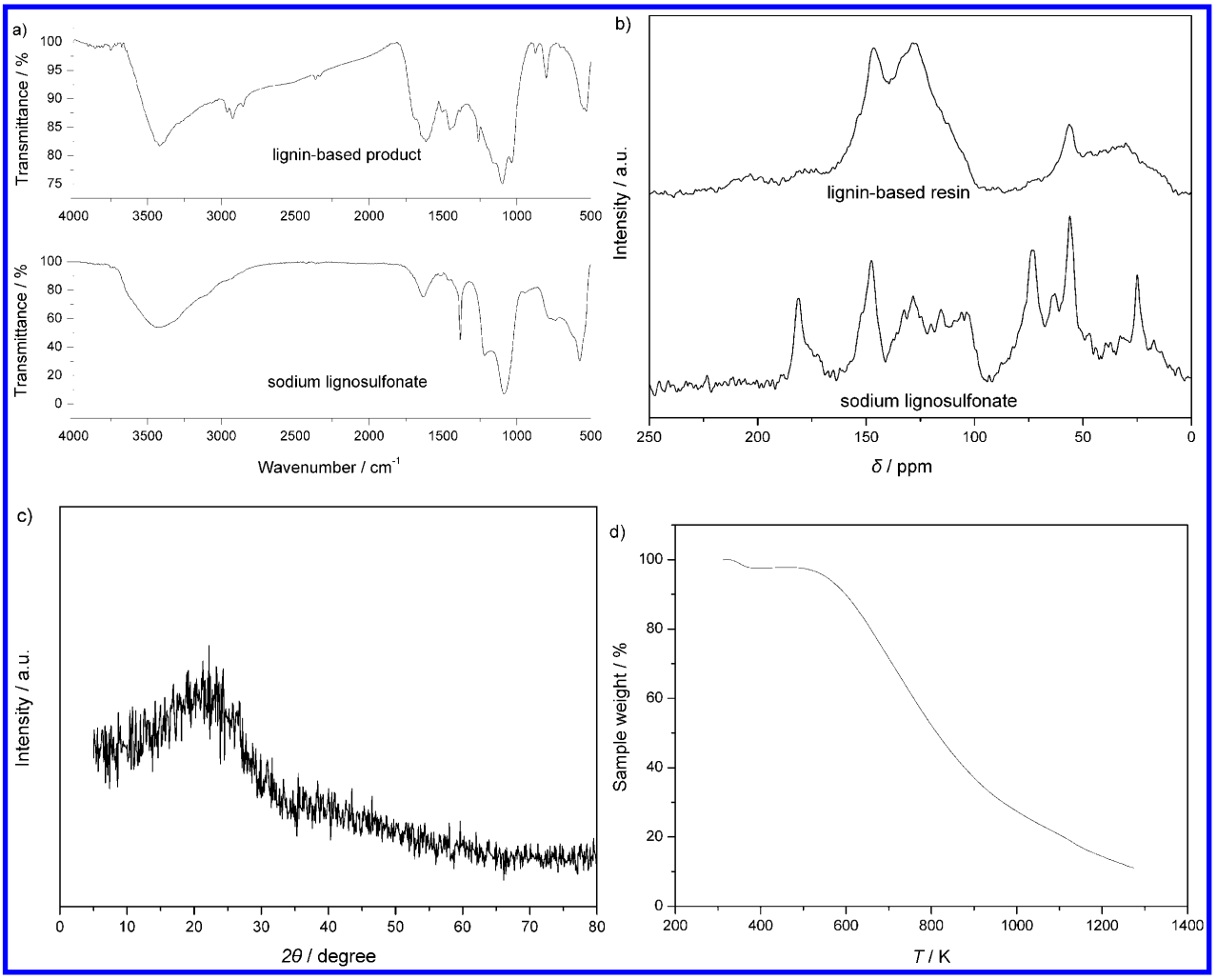

Figure 3. (a) FTIR spectra, (b) ^{13}C MAS NMR spectra, (c) powder XRD pattern, and (d) TGA trace of the SLS precursor and LBR.

The XRD pattern (Figure 3c) for LBR exhibits two broad, weak diffraction peaks (2θ = 10°−30°, 35°−50°) that are attributable to amorphous cross-linked phenylpropane-based polymers oriented in a random fashion.[15] The total exchange capacity of LBR was determined by the titration (see Table 1).

Table 1. Characteristic Properties of LBR

resin type	lignin-based resin (LBR)	Amberlite IRC-50
ionic form	H^+	H^+
matrix	lignin	acrylic polymer
functional groups	COOH/COOR/OH	COOH
total exchange capacity	4.1 mmol/g	10.0 mmol/g
specific surface area	13−20 m^2/g	43−53 m^2/g

According to XPS analysis, no S atoms have been found in LBR, suggesting that no SO_3H groups are present in the samples. Thus, based on reaction bases for Boehm titration—that is, sodium hydrogen carbonate neutralizes only carboxyl groups on the polymers surface, sodium carbonate neutralizes carboxyls and lactones, and sodium hydroxide neutralizes carboxyls, lactones, and phenolic groups—the amount of carboxyl groups was 2.6 mmol/g, which decreased to 1.0 mmol/g for phenolic groups, and 0.5 mmol/g for lactone groups. Moreover, the amount of acid sites per unit surface area for LBR is comparable to that of Amberlite IRC-50. These results indicate that the solid resin consisting of amorphous phenylpropane-based polymers with attached acidic groups can function as an acidic resin with a high density of acid sites.

3.3. Stability. The thermal stability of LBR was examined by TGA. The TGA trace (Figure 3d) showed that the sample weight decreased with increasing temperature, reaching a plateau at 383 K. The weight loss observed in the temperature range of 328−383 K can be attributed to the loss of water, indicating that the moisture content of LBR is only 2.5%. A further decrease in weight was observed upon heating above 520 K, which was due to the breakdown of ether linkages and scission of aromatic side chains in LBR.[16] Therefore, the thermal stability of the material is not inferior to that of Amberlite IRC-50, which begins to decompose at ∼523 K.

3.4. Adsorption Performance. The strength and density of acid sites on LBR were demonstrated through adsorption behavior of heavy-metal ions. In the present study, adsorption properties of heavy metals on LBR were studied using aqueous solutions containing Cr(III), Cu(II), Ni(II), Pb(II), and Cd(II) ions as typical examples. The effects of pH, LBR dosage, and contact time on adsorption were investigated using batch experiments. Experimental results were analyzed and fitted by equilibrium isotherms and kinetic models. Moreover, the regeneration method of LBR was studied.

3.4.1. Effect of pH. According to the previous studies,[17,18] pH is an important factor governing the adsorption behavior of

dx.doi.org/10.1021/ie301863e | Ind. Eng. Chem. Res. 2013, 52, 1267−1274

metal ions, because of its effect on the surface charge of adsorbent and the degree of ionization. The effect of pH on adsorption of Cr(III), Cu(II), Ni(II), Pb(II), and Cd(II) by LBR was studied at different pH values ranging from 2 to 8, and the results are shown in Figure 4. As pH increases, the

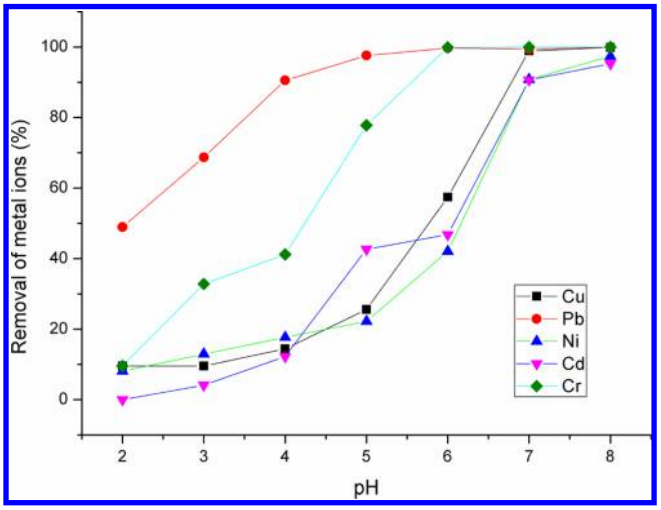

Figure 4. Effect of pH on removal efficiency of heavy-metal ions by LBR.

adsorbent surface becomes more negatively charged, thus, facilitating greater removal efficiency.[18] On the other hand, calculated from solubility products (K_{sp}), formation of metal hydroxides occurs at pH 6.2 for Cu(II), pH 7.5 for Pb(II), pH 7.6 for Ni(II), pH 8.3 for Cd(II), and pH 5.3 for Cr(III) with an initial metal concentration of 200 mg/L. When pH value goes beyond the pH threshold of metal precipitation, the removal process could be considered as a combination of adsorption and precipitation of metal hydroxides. Therefore, to eliminate the effect of metal precipitation and compare the results of experimental studies, all further adsorptions of Cu(II), Ni(II), Pb(II), Cd(II), and Cr(III) were conducted at pH values of 6.0, 6.0, 6.0, 6.0, and 5.0, respectively.

3.4.2. Effect of LBR Dose. The adsorption of heavy metals, as a function of LBR dosage, was studied. The experiments were conducted with the given LBR dose at the initial concentration of 200 mg/L. As shown in Figure 5, the removal of all metal

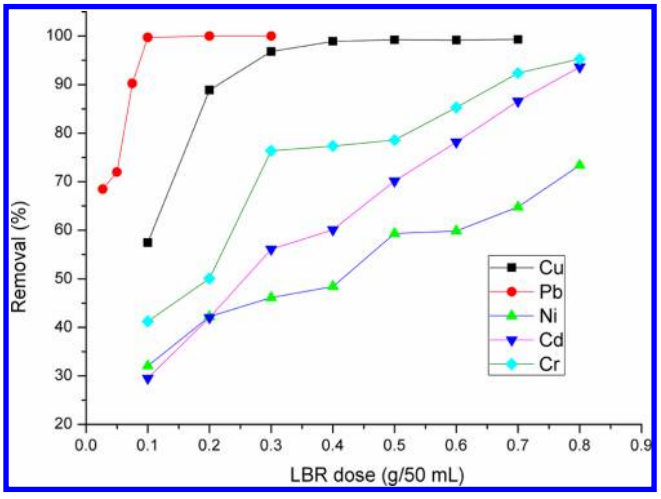

Figure 5. Removal of metal ions, as a function of adsorbent loading.

ions increased as the adsorbent loading increased at the given metal ion concentration until the maximum adsorption efficiencies (100%) were obtained, which was attributable to increase the surface area and the number of sites with increasing of LBR dose.[19] However, the equilibrium adsorption capacities (q_e) decreased as the loading of LBR mass was increased from 0.1 g/50 mL to 0.8 g/50 mL, because of an increase in the ratio of adsorbent to adsorbate.[20,21] Furthermore, according to the previous study,[18] a fixed quantity of adsorbent can only offer a finite number of active sites; thus, the optimal adsorbent dose for adsorption should depend directly on the initial concentrations of metal ions. Thus, in order to facilitate analysis and comparison of the experimental data, the remaining experiments were performed with 0.2 g/50 mL for Pb(II), 0.3 g/50 mL for Cu(II), 0.3 g/50 mL for Ni(II), 0.3 g/50 mL for Cd(II), and 0.3 g/50 mL for Cr(III), with an initial metal concentration of 200 mg/L.

3.4.3. Effect of Contact Time. As shown in Figure 6, the removal of heavy metals by LBR as a function of contact time

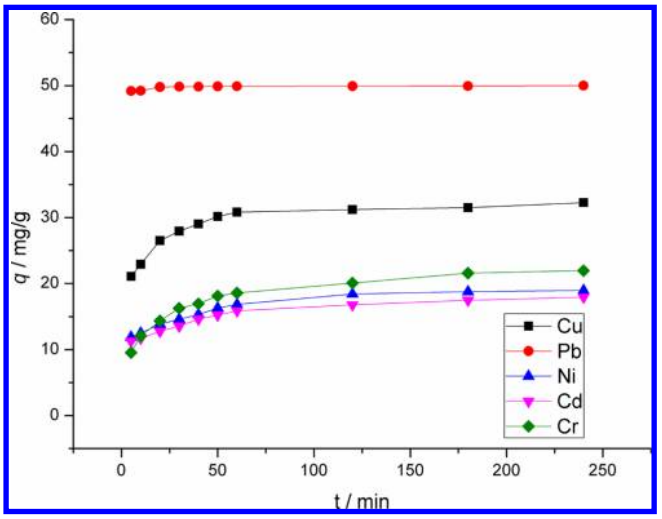

Figure 6. Adsorption of Cu(II), Ni(II), Pb(II), Cd(II), and Cr(III) on LBR at different contact times.

was investigated. Contact time was varied in the range of 5–240 min. The value of q increased as the contact time increased, until equilibrium was reached. The adsorption of Pb on LBR was rapid for the first 10 min and reached equilibrium within 20 min. However, in contrast with the removal of Pb, the removal of the other metal ions was relatively lower, and the processes reached equilibrium within 60 min. Therefore, the period of 60 min was considered as the optimum time.

3.4.4. Analysis of Adsorption Isotherms. The equilibrium adsorption isotherms are important to describe the relationship between equilibrium metal uptake (q_e, mg/g) and equilibrium concentration of metal ions in solution (C_e, mg/L). Various sorption isotherm models are well-known and widely employed for fitting the data. In the present work, two-parameter isotherm models, such as the Langmuir, Freundlich, and Dubinin–Radushkevich (D-R) isotherms, are selected to be studied.

The Langmuir isotherm[22] is given as

$$q_e = \frac{q_m b C_e}{1 + b C_e} \quad (5)$$

dx.doi.org/10.1021/ie301863e | Ind. Eng. Chem. Res. 2013, 52, 1267–1274

where q_m is the maximal adsorption capacity (mg/g) and b is the Langmuir constant of the system (L/mg). The constants, q_m and b are usually evaluated from the plot of the following linear equation:

$$\frac{C_e}{q_e} = \frac{C_e}{q_m} + \frac{1}{q_m b} \quad (6)$$

The Freundlich model[22] can be described by eq 7,

$$q_e = K_F C_e^{1/n} \quad (7)$$

or its logarithmic form:

$$\log q_e = \log K_F + \left(\frac{1}{n}\right)\log C_e \quad (8)$$

where K_F is a constant relating the adsorption capacity (mg/g) and $1/n$ is an empirical parameter related to the adsorption intensity. The value of K_F and $1/n$ are found by plotting the graph between log q_e and log C_e.

The Dubinin−Radushkevich (D-R) isotherm equation[23] can by written as

$$q_e = q_m \exp(-Be^2) \quad (9)$$

or its linearized form:

$$\ln q_e = \ln q_m - Be^2 \quad (10)$$

where e is the Polanyi potential, which can be worked out by eq 11:

$$e = RT \ln\left(1 + \frac{1}{C_e}\right) \quad (11)$$

where R is the gas constant (8.314 J/(mol K)), and T is the absolute temperature (K). The D-R parameters (q_m and B) are calculated from the plot of ln q_e versus e^2. B is an activity coefficient related to the mean free energy of adsorption per mole of the adsorbate; this energy (E) can be defined as

$$E = \frac{1}{\sqrt{2B}} \quad (12)$$

The experimental data were fitted by the two-parameter models. The correlation coefficients (R^2) and isotherm parameters are presented in Table 2. The values of R^2 as indicators were used to assess the goodness of fit.[24] The values of R^2 for Cu, Pb, and Cr are 0.997, 0994, and 0.960, respectively, indicating that the Langmuir models give a good fit to the adsorption data of Cu, Pb, and Cr onto LBR. However, the better fit to experimental data for Ni and Cd was provided by the Freundlich model, as indicated by the R^2 values of 0.990 and 0.950 for Ni and Cd, respectively. The D-R isotherm model was unable to fit the experimental data because low correlation coefficients were observed. Thus, Langmuir and Freundlich isotherms exhibited good fits to the experimental adsorption data and gave good ideas about the sorption mechanism. According to the results from the D-R model, the E values are 0.869 kJ/mol for Cu(II), 0.118 kJ/mol for Pb(II), 0.0236 kJ/mol for Ni(II), 0.0461 kJ/mol for Cd(II), and 0.0593 kJ/mol for Cr(III), which indicate that the adsorption process is endothermic and that the removal of heavy metals is mostly through physical adsorption.[22,23] The maximum equilibrium adsorption capacity was obtained from the Langmuir equation fitting for Pb(II) (194.553 mg/g), which decreased to 59.998 mg/g for Cu(II), 48.80 mg/g for Cd(II), 42.450 mg/g for Ni(II), and 41.847 mg/g for Cr(III). The adsorption of Pb is preferential compared to the other metals, attributed to the fact that two main types of acid sites (carboxylic- and phenolic-type surface groups) on LBR have a higher affinity for Pb(II) than the other metal ions.[25−27] Therefore, LBR has affinity with metal ions in the following order: Pb(II) ≫ Cu(II) > Cd(II) > Ni(II) ≈ Cr(III). The predicted maximum adsorption capacity for Cr(III) is 122% more than the result obtained by Mustafa for Cr(III) adsorption on Amberlite IRC-50,[28] suggesting that LBR has the potential to replace commercial ion-exchange resin in metal ion separation and remediation. Furthermore, the q_m values for Cu(II), Ni(II), Pb(II), and Cd(II) using LBR were greater than the other lignin materials reported in the previous literatures.[27,29] Therefore, LBR exhibits a high activity for the removal of heavy metals from aqueous solutions.

Table 2. Summary of Adsorption Isotherm Parameters for LBR

	Metal				
parameter	Cu(II)	Pb(II)	Ni(II)	Cd(II)	Cr(III)
Langmuir					
R^2	0.997	0.994	0.921	0.930	0.960
q_m(mg/g)	59.988	194.553	42.450	48.80	41.847
b(L/mg)	0.217	0.343	0.00406	0.00719	0.0267
Freundlich					
R^2	0.974	0.839	0.990	0.951	0.903
n	3.915	13.560	1.407	1.914	2.763
K_F(mg/g)	19.311	102.360	0.445	1.755	4.663
D-R					
R^2	0.871	0.705	0.668	0.527	0.602
q_m(mg/g)	44.690	203.718	24.845	25.518	32.344
B(kJ^2/mol^2)	0.662	36.102	895.192	235.324	142.342
E(kJ/mol)	0.869	0.118	0.0236	0.0461	0.0593

3.4.5. Analysis of Adsorption Kinetics. In order to analyze the adsorption kinetics of heavy metals, three kinetic models (pseudo-first-order, pseudo-second-order, and intraparticle diffusion model) were used to test the experimental data. The pseudo-first-order expression[30] is given as

$$q_t = q_e[1 - \exp(-k_1 t)] \quad (13)$$

and the pseudo-second-order equation[31] is expressed in the following form:

$$q_t = \frac{k_2 q_e^{\ 2} t}{1 + k_2 q_e t} \quad (14)$$

where q_e is the adsorption capacity at equilibrium (mg/g), q_t the adsorption capacity at time t (min), k_1 the first-order rate constant (1/min), and k_2 the second-order rate constant (mg/(g min)).

Furthermore, the intraparticle diffusion model[23] can be expressed by the following equations:

$$q_t = k_p t^{0.5} \quad (15)$$

where k_p is the rate constant (mg/g min$^{-1/2}$), which can be calculated from the slope between q_t vs $t^{0.5}$.

The rate constants of the kinetic models (q_e) and the correlation coefficient (R^2) values were calculated and are listed in Table 3. The R^2 values for the pseudo-second-order model are relatively higher than that of the other kinetic models.

dx.doi.org/10.1021/ie301863e | Ind. Eng. Chem. Res. 2013, 52, 1267−1274

Table 3. Fitting of Kinetic Models for Adsorption of Heavy Metals on LBR

		Pseudo-first-order			Pseudo-second-order			Intraparticle diffusion	
metal	$q_{e\ (exp)}$ (mg/g)	k_1 (1/min)	q_e (mg/g)	R^2	k_2 (g/mg min)	q_e (mg/g)	R^2	k_p(mg/g $min^{-1/2}$)	R^2
Cu	32.267	0.189	29.981	0.686	0.00986	31.848	0.938	2.977	0.354
Pb	50	0.868	49.811	0.791	0.216	49.957	0.945	5.042	0.691
Ni	18.965	0.179	16.708	0.823	0.0137	18.109	0.976	1.719	0.420
Cd	17.931	0.185	15.580	0.792	0.0151	16.868	0.957	1.644	0.288
Cr	21.952	0.083	19.539	0.768	0.00544	21.652	0.950	1.924	0.688

Similarly, the q_e values calculated using the pseudo-second-order kinetic model are very close to the experimental values ($q_{e(exp)}$). Accordingly, the adsorption of heavy metals on LBR is well-described by the pseudo-second-order model. Based on the plot of q_t vs $t^{0.5}$ (see Figure 7), the adsorption is comprised

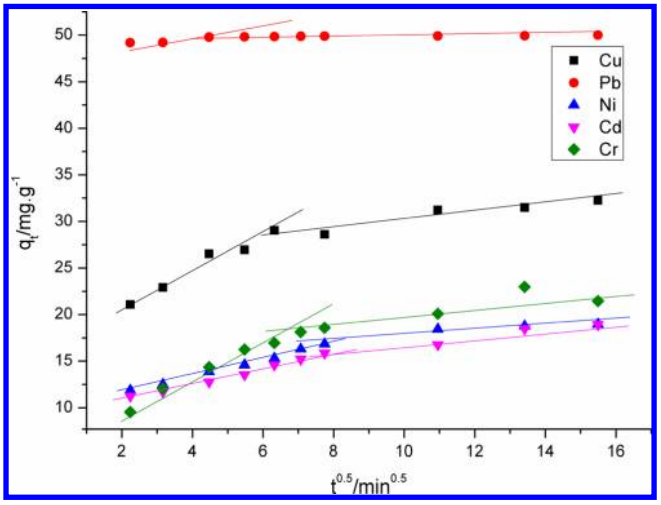

Figure 7. Intraparticle diffusion plot for the adsorption of metals on LBR.

of two stages, indicating that the intraparticle diffusion was not the rate-determining step for the entire process.[32] Therefore, according to the fact that the adsorption process is mostly through physical adsorption, it can be argued that film diffusion process is the rate-controlling step in the adsorption process.[23] Moreover, based on the pseudo-second-order model, the initial adsorption rate v_0 calculated as $v_0 = kq_e^2$ was in the following sequence: Pb(II) ≫ Cu(II) > Ni(II) ≈ Cd(II) > Cr(III). This result is consistent with the known facts shown in Figure 6.

3.4.6. Regeneration of LBR. The reusability of an effective and low-cost adsorbent is especially important to the commercialization. Thus, the adsorption/desorption ability of LBR was examined. In the present study, 0.5 mol/L hydrochloric acid (HCl) was selected as the desorption agent to regenerate the spent LBR with metal ions, because of the fact that HCl has the high desorption efficiency and is the most commonly used for the regeneration of the exhausted adsorbent.[22,33]

Figure 8 shows desorption capability of LBR for all metal ions after each adsorption/desorption cycle. The uptake capacity for Pb(II), Cu(II), Ni(II), and Cd(II) had a slight decrease in four cycles, but the highest reduction in adsorption capacity was noticed for Cr(III). For Cr(III), in the first desorption, a lowest desorption efficiency of 13.35% was achieved. During the second adsorption, the adsorption capacity (2.195 mg/g) is only 10% of the capacity in the first adsorption, because there are fewer available adsorption sites

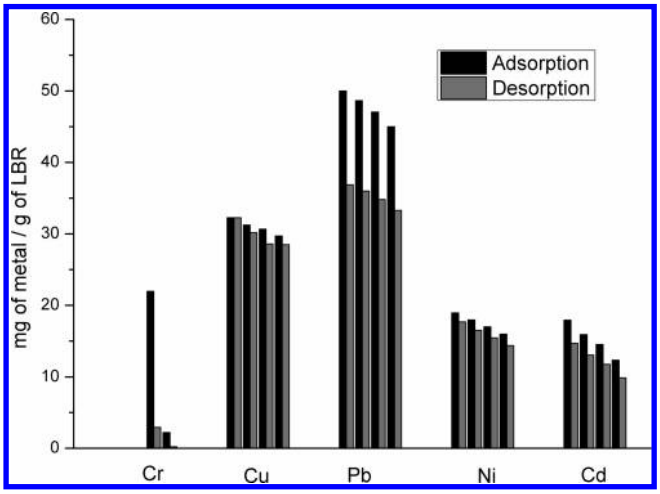

Figure 8. Adsorption/desorption cycles for LBR with all metal ions.

on the adsorbent surface, while a large number of the adsorption sites were occupied with the residual Cr(III) ions after desorption. However, the average desorption efficiencies for four cycles were 98.23%, 90.28%, 80.03%, and 71.75% for Cu(II), Ni(II), Cd(II), and Pb(II), respectively, attributing it to ion exchange between the hydrogen ions from the desorption mineral acids (HCl) and the adsorbed metal ions onto LBR.[18] Under the same experimental conditions, thus, the metal-ion-binding strength on the adsorbent might be quantified by the desorption efficiency; the greater the metal-ion-binding strength, the lower the desorption efficiency. Therefore, the strengths of the five metal ions binding with LBR are in the following order: Cr(III) ≫ Pb(II) > Cd(II) > Ni(II) > Cu(II).

4. CONCLUSIONS

In the present study, sodium lignosulfonates was used to synthesis a new lignin-based ion-exchange resin (LBR) by condensation polymerization with glucose under acidic conditions. The resulting spherical material is consisting of amorphous cross-linked phenylpropane-based polymers with high density of acid sites. The use of LBR for the removal of Cr(III), Cu(II), Ni(II), Pb(II), and Cd(II) ions from aqueous solutions at room temperature have also been examined. Experimental data for Cu, Pb, and Cr perfectly fitted the Langmuir model, but the better fit to experimental data on the adsorption of Ni and Cd was provided by the Freundlich model. The maximum adsorption capacity (q_m) for Pb(II) is 194.553 mg/g, which decreased to 59.998 mg/g for Cu(II), 48.80 mg/g for Cd(II), 42.450 mg/g for Ni(II), and 41.847 mg/g for Cr(III). Therefore, LBR exhibits high activity for the removal of heavy-metal ions and has clear potential for use as a replacement for petroleum-based resins. The kinetic data shows that the adsorption of heavy metals fits better with the pseudo-second-order kinetic model than other models. Moreover, the

dx.doi.org/10.1021/ie301863e | Ind. Eng. Chem. Res. 2013, 52, 1267−1274

metal-loaded LBR can be easily regenerated and reused by a simple acid treatment, except for LBR with the adsorbed chromium.

AUTHOR INFORMATION

Corresponding Author

*Tel: +86-10-6441-2054. Fax: +86-10-6441-9619. E-mail: huangcp@mail.buct.edu.cn.

Notes

The authors declare no competing financial interest.

ACKNOWLEDGMENTS

This project was sponsored by the National Natural Science Foundation of China (under Grant No. 20806007) and the National Basic Research Program of China (973 Program) (No. 2010CB226902).

REFERENCES

(1) Sahu, S. K.; Meshram, P.; Pandey, B. D.; Kumar, V.; Mankhand, T. R. Removal of chromium(III) by cation exchange resin, Indion 790 for tannery waste treatment. *Hydrometallurgy* **2009**, *99*, 170−174.

(2) Ding, J.; He, B.; Li, J. Cation ion-exchange resin/polyethersulfone hybrid catalytic membrane for biodiesel production. *J. Biobased Mater. Bioenergy* **2011**, *5*, 85−91.

(3) Honkela, M. L.; Root, A.; Lindblad, M.; Krause, A. O. I. Comparison of ion-exchange resin catalysts in the dimerisation of isobutene. *Appl. Catal., A* **2005**, *295*, 216−223.

(4) Mungroo, R.; Pradhan, N. C.; Goud, V. V.; Dalai, A. K. Epoxidation of canola oil with hydrogen peroxide catalyzed by acidic ion exchange resin. *J. Am. Oil Chem. Soc.* **2008**, *85*, 887−896.

(5) Zakzeski, J.; Bruijnincx, P. C. A.; Jongerius, A. L.; Weckhuysen, B. M. The Catalytic Valorization of Lignin for the Production of Renewable Chemicals. *Chem. Rev.* **2010**, *110*, 3552−3599.

(6) Gosselink, R. J. A.; de Jong, E.; Guran, B.; Abächerli, A. Co-ordination network for lignin−standardisation, production and applications adapted to market requirements (EUROLIGNIN). *Ind. Crops Prod.* **2004**, *20*, 121−129.

(7) Rao, G. V.; Jagannadhan, V.; Venkatasubramanian, N. Utilization of lignin and its derivatives for industrial purpose. *Ind. Pulp Pap.* **1978**, *6*, 11−15.

(8) Liu, M. H.; Zhan, H. Y.; Liu, Q. J.; Chen, F. G. Preparation of spherical lignin beads and study on their particle size distribution. *J. Cell. Sci. Technol.* **2003**, *11*, 8−13.

(9) Fan, J.; Zhan, H. Y.; Yin, Q. W.; Liu, M. H. Study on preparation and fundamental characteristics of spherical lignin-based ion exchange resin. *China Pulp Pap.* **2005**, *24*, 18−22.

(10) Oickle, A. M.; Goertzen, S. L.; Hopper, K. R.; Abdalla, Y. O.; Andreas, H. A. Standardization of the Boehm titration: Part II. Method of agitation, effect of filtering and dilute titrant. *Carbon* **2010**, *48*, 3313−3322.

(11) Goertzen, S. L.; Theriault, K. D.; Oickle, A. M.; Tarasuk, A. C.; Andreas, H. A. Standardization of the Boehm titration. Part I. CO_2 expulsion and endpoint determination. *Carbon* **2010**, *48*, 1252−1261.

(12) Balakshin, M. Y.; Capanema, E. A.; Goldfarb, B.; Frampton, J.; Kadla, J. F. NMR studies on Fraser fir *Abies fraseri* (Pursh) Poir. lignins. *Holzforschung* **2005**, *59*, 488−496.

(13) Holtman, K. M.; Chang, H.-M.; Jameel, H.; Kadla, J. F. Quantitative ^{13}C NMR characterization of milled wood lignins isolated by different milling techniques. *J. Wood Chem. Technol.* **2006**, *26*, 21−34.

(14) McKenzie, B. F. Levulinic acid. *Org. Synth.* **1941**, *1*, 335.

(15) Hara, M.; Yoshida, T.; Takagaki, A.; Takata, T.; Kondo, J.; Hayashi, S.; Domen, K. A carbon material as a strong protonic acid. *Angew. Chem. Int. Ed.* **2004**, *43*, 2955−2958.

(16) Jiang, G.; Nowakowski, D. J.; Bridgwater, A. V. A systematic study of the kinetics of lignin pyrolysis. *Thermochim. Acta* **2010**, *498*, 61−66.

(17) El-Ashtoukhy, E. S. Z.; Amin, N. K.; Abdelwahab, O. Removal of lead(II) and copper(II) from aqueous solution using pomegranate peel as a new adsorbent. *Desalination* **2008**, *223*, 162−173.

(18) Javaid, A.; Bajwa, R.; Shafique, U.; Anwar, J. Removal of heavy metals by adsorption on *Pleurotus ostreatus*. *Biomass Bioenergy* **2011**, *35*, 1675−1682.

(19) Bansal, M.; Singh, D.; Garg, V. K. A comparative study for the removal of hexavalent chromium from aqueous solution by agriculture wastes' carbons. *J. Hazard. Mater.* **2009**, *171*, 83−92.

(20) Sari, A.; Mendil, D.; Tuzen, M.; Soylak, M. Biosorption of Cd(II) and Cr(III) from aqueous solution by moss (*Hylocomium splendens*) biomass: Equilibrium, kinetic and thermodynamic studies. *Chem. Eng. J.* **2008**, *144*, 1−9.

(21) Moussavi, G.; Barikbin, B. Biosorption of chromium(VI) from industrial wastewater onto pistachio hull waste biomass. *Chem. Eng. J.* **2010**, *162*, 893−900.

(22) Lasheen, M. R.; Ammar, N. S.; Ibrahim, H. S. Adsorption/desorption of Cd(II), Cu(II) and Pb(II) using chemically modified orange peel: Equilibrium and kinetic studies. *Solid State Sci.* **2012**, *14*, 202−210.

(23) Dlamini, D. S.; Mishra, A. K.; Mamba, B. B. Kinetic and equilibrium studies of the removal of Pb^{2+} from aqueous solutions using Na_2SO_4-EVA/Cloisite 20A composite. *Mater. Chem. Phys.* **2012**, *133*, 369−375.

(24) Revathi, M.; Saravanan, M.; Chiya, A. B.; Velan, M. Removal of Copper, Nickel, and Zinc Ions from Electroplating Rinse Water. *Clean-Soil Air Water* **2012**, *40*, 66−79.

(25) Ravat, C.; Dumonceau, J.; Monteil-Rivera, F. Acid/base and Cu(II) binding properties of natural organic matter extracted from wheat bran: modeling by the surface complexation model. *Water Res.* **2000**, *34*, 1327−1339.

(26) Ravat, C.; Monteil-Rivera, F.; Dumonceau, J. Metal ions binding to natural organic matter extracted from wheat bran: Application of the surface complexation model. *J. Colloid Interface Sci.* **2000**, *225*, 329−339.

(27) Guo, X.; Zhang, S.; Shan, X.-q. Adsorption of metal ions on lignin. *J. Hazard. Mater.* **2008**, *151*, 134−142.

(28) Mustafa, S.; Shah, K. H.; Naeem, A.; Waseem, M.; Tahir, M. Chromium(III) removal by weak acid exchanger Amberlite IRC-50 (Na). *J. Hazard. Mater.* **2008**, *160*, 1−5.

(29) Wu, Y.; Zhang, S.; Guo, X.; Huang, H. Adsorption of chromium(III) on lignin. *Bioresour. Technol.* **2008**, *99*, 7709−7715.

(30) Ho, Y. S. Citation review of Lagergren kinetic rate equation on adsorption reactions. *Scientometrics* **2004**, *59*, 171−177.

(31) Ho, Y. S. Second-order kinetic model for the sorption of cadmium onto tree fern: A comparison of linear and non-linear methods. *Water Res.* **2006**, *40*, 119−125.

(32) Khambhaty, Y.; Mody, K.; Basha, S.; Jha, B. Kinetics, equilibrium and thermodynamic studies on biosorption of hexavalent chromium by dead fungal biomass of marine *Aspergillus niger*. *Chem. Eng. J.* **2009**, *145*, 489−495.

(33) Zan, F. Y.; Huo, S. L.; Xi, B. D.; Zhao, X. L. Biosorption of Cd^{2+} and Cu^{2+} on immobilized *Saccharomyces cerevisiae*. *Front. Environ. Sci. Eng. China* **2012**, *6*, 51−58.